Electron Emission from Diamondoids: A Diffusion Quantum Monte Carlo Study

N. D. Drummond,[1] A. J. Williamson,[2,*] R. J. Needs,[1] and G. Galli[2]

[1]*TCM Group, Cavendish Laboratory, University of Cambridge, Cambridge CB3 0HE, United Kingdom*
[2]*Lawrence Livermore National Laboratory, Livermore, California 94550, USA*

(Received 14 February 2005; published 22 August 2005)

We present density-functional theory (DFT) and quantum Monte Carlo (QMC) calculations designed to resolve experimental and theoretical controversies over the optical properties of H-terminated C nanoparticles (diamondoids). The QMC results follow the trends of well-converged plane-wave DFT calculations for the size dependence of the optical gap, but they predict gaps that are 1–2 eV higher. They confirm that quantum confinement effects disappear in diamondoids larger than 1 nm, which have gaps below that of bulk diamond. Our QMC calculations predict a small exciton binding energy and a negative electron affinity (NEA) for diamondoids up to 1 nm, resulting from the delocalized nature of the lowest unoccupied molecular orbital. The NEA suggests a range of possible applications of diamondoids as low-voltage electron emitters.

DOI: 10.1103/PhysRevLett.95.096801 PACS numbers: 73.22.−f, 02.70.Ss, 71.15.Mb

Designing the nanoscale building blocks for future nanotechnological devices is one of the most rapidly evolving fields of materials science. In the area of nanoscale optoelectronic materials, attention was originally focused on semiconductor nanoparticles constructed from Si [1] or Ge [2], as these nanoparticles can easily be integrated with existing Si fabrication techniques. Recently, however, it was discovered that large quantities of high-quality, H-terminated C nanoparticles can be isolated from petroleum and separated into monodisperse samples [3]. These *diamondoids* are expected to have several technologically useful optoelectronic properties. In particular, the effect of quantum confinement is expected to push diamondoid optical gaps into the UV range, enabling a unique set of sensing applications. Additionally, it has been demonstrated [4,5] that H-terminated diamond surfaces exhibit negative electron affinities (NEAs), suggesting that diamondoids will also have NEAs. This opens up the possibility of coating surfaces with diamondoids to produce new electron-emission devices.

The breakthrough in isolating diamondoids has sparked interest in measuring [6–8] and calculating their structural and optoelectronic properties [7,9–12]. However, such studies have proved to be challenging and have produced several controversial results. In 1999, the results of x-ray absorption near-edge structure studies of diamond films produced by chemical vapor deposition (CVD) [6] were used to infer the evolution of the nanoparticle gap with size. This showed a persistence of quantum confinement effects up to 27 nm, much longer than in Si or Ge nanoparticles, where quantum confinement effects disappear above 5–7 nm. In contrast, recent near-edge absorption fine structure studies of diamondoids prepared by hot-filament CVD [13] and high-explosive detonation waves [7] showed that quantum confinement effects disappear in particles larger than 4 nm.

Theoretical models for the optoelectronic properties of diamondoids have also produced contradictory results. Raty *et al.* [7] studied the size dependence of the optical gap using both time-independent and time-dependent density-functional theory (DFT) calculations, and concluded that quantum confinement effects disappear in nanoparticles larger than 1 nm. Raty *et al.* [7] also predicted that the gaps of diamondoids with sizes between 1 and 1.5 nm are *below* the gap of bulk diamond. This is strikingly different to the behavior of H-terminated Si and Ge nanoparticles, for which the gaps are always above the bulk band gap [14]. In contrast, recent DFT calculations by McIntosh *et al.* [12] for the same particles predict optical gaps 2 eV above the gap of bulk diamond for particles ranging in size from 0.5 to 2 nm.

In this Letter, we resolve these controversies by performing both DFT and highly accurate quantum Monte Carlo (QMC) calculations to predict the size dependence of the optical gap and the electron affinity of diamondoids. We have studied two classes of nanoparticles: (i) diamondoids constructed from adamantane cages, *adamantane*, $C_{10}H_{16}$, *diamantane*, $C_{14}H_{20}$, and *pentamantane*, $C_{26}H_{32}$; (ii) H-terminated, spherical, diamond-structure nanoparticles, $C_{29}H_{36}$, $C_{66}H_{64}$, and $C_{87}H_{76}$. The nanoparticle sizes and symmetries are given in Table I. Because diamondoids can be extracted in large quantities from petroleum and highly purified using high-pressure liquid chromatography, we anticipate that actual experimental samples will consist largely of the high-symmetry structures studied in this work. This is not the case for Si and Ge nanoparticles, where limitations in current synthesis techniques prevent the routine production of high-symmetry nanoparticles.

Our DFT calculations were performed using both plane-wave and Gaussian basis sets. The Perdew-Burke-Ernzerhof (PBE) [16] functional was used in all the DFT calculations, as this has been shown to reproduce accurately the structural and electronic properties of diamond [7]. The plane-wave calculations were performed with the GP [17], QBox [18], and ABINIT [19] codes. A plane-wave

TABLE I. Point-group symmetry, size (in nm), DFT and DMC optical gaps, DMC electron affinities (EA), and DMC ionization potentials (IP) (all in eV) of different diamondoids.

Cluster	Symmetry	Size	DFT gap	DMC gap	EA	IP
$C_{10}H_{16}$	T_d	0.50	5.77	7.61(2)	−0.13(2)	10.15(3)
$C_{14}H_{20}$	D_{3d}	0.69	5.41	7.32(3)		
$C_{26}H_{32}$	T_d	0.74	5.03	7.04(6)		
$C_{29}H_{36}$	T_d	0.76	4.90	6.67(6)	−0.29(6)	7.63(5)
$C_{66}H_{64}$	T_d	1.00	4.37	5.09(18)		
$C_{87}H_{76}$	T_d	1.14	3.94			
Diamond			4.23 [7]	5.6(2) [15]		

cutoff of 55 Ry and a cubic simulation cell of side length 30 Å were used for all calculations. Norm-conserving Troullier-Martins (TM) pseudopotentials were used to represent the ionic cores. The all-electron Gaussian calculations were performed with the G03 code [20].

The initial structures of $C_{10}H_{16}$, $C_{14}H_{20}$, and $C_{26}H_{32}$ were taken from Ref. [3], while those of $C_{29}H_{36}$, $C_{66}H_{64}$, and $C_{87}H_{76}$ were constructed from the bulk-diamond structure, and the C-H bond lengths were set to the experimental value in CH_4. All the structures were fully relaxed to their lowest-energy configurations within DFT before their electronic and optical properties were calculated. For $C_{10}H_{16}$, $C_{14}H_{20}$, and $C_{26}H_{32}$, DFT-PBE calculations predict small relaxations in the bond lengths and angles, similar to Ref. [12] The C-C and C-H bond lengths are 1.55 and 1.10 Å, respectively, essentially identical to the bulk-diamond and methane bond lengths. The bond angles vary from 108.5° to 110.5°. For the larger, spherical particles ($C_{29}H_{36}$, $C_{66}H_{64}$, and $C_{87}H_{76}$), DFT-PBE calculations predict a 3%–4% increase in the C-C bond lengths, while the C-H bonds remain at 1.10 Å. The bond angles vary from 102° to 113°.

The results of our DFT calculations for the single-particle states of the diamondoids are shown in Fig. 1 and listed in Table I. Figure 1(a) shows the size dependence of the DFT eigenvalue gap between the highest occupied molecular orbital (HOMO) and the lowest unoccupied molecular orbital (LUMO), calculated using the plane-wave basis set described above. All the HOMO-LUMO gaps are converged with respect to the size of the supercell and the plane-wave basis. The HOMO-LUMO gap decreases as the size of the nanoparticles increases. For nanoparticles larger than 1 nm, the DFT-PBE HOMO-LUMO gap is smaller than the DFT-PBE gap of bulk diamond.

Figure 1(b) shows the size dependence of the individual DFT HOMO and LUMO eigenvalues. When the size of the nanoparticles is reduced, the HOMO eigenvalue decreases continuously, as predicted by standard models of quantum confinement [21]. The lower symmetry of $C_{14}H_{20}$ does not alter the trend in the HOMO eigenvalue. In contrast, the LUMO eigenvalue displays almost no quantum confinement and is nearly independent of size. This behavior differs from that of H-terminated Si and Ge nanoparticles [14], in which both the HOMO and LUMO exhibit clear quantum confinement.

The origin of the anomalous size dependence of the LUMO energy can be understood by comparing the HOMO and the LUMO. Figure 2 shows isosurfaces of the HOMO and LUMO of $C_{29}H_{36}$. The HOMO is localized on the C-C and C-H covalent bonds inside the nanoparticle, while the LUMO is a delocalized state with considerable charge outside of the H atoms terminating the surface. As the size of the nanoparticles increases, one expects the HOMO to evolve smoothly into the valence-band maximum of bulk diamond. In contrast, for larger diamondoids, the LUMO remains localized on the surface and is closer in

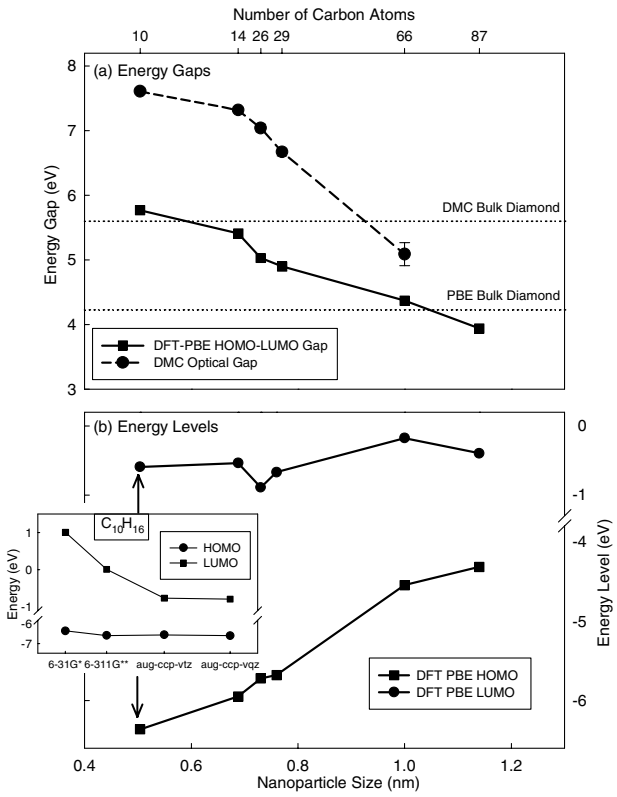

FIG. 1. Calculated size dependence of (a) DFT HOMO-LUMO gap and DMC optical gap, and (b) DFT HOMO and LUMO eigenvalues. The inset shows the convergence of the DFT HOMO and LUMO eigenvalues with basis set.

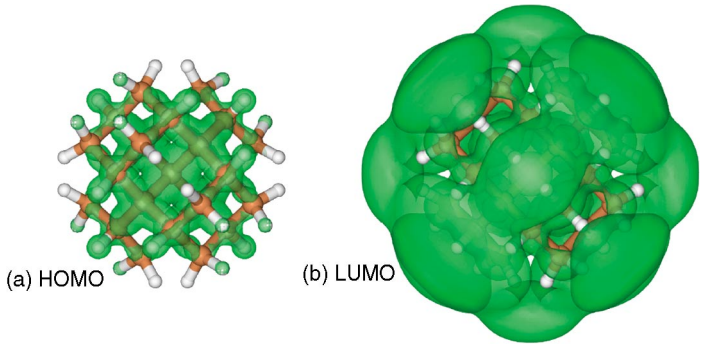

FIG. 2 (color). Isosurface plots of the square of the (a) HOMO and (b) LUMO of $C_{29}H_{36}$. The green isosurfaces include 50% of the charge in each orbital.

nature to a defect or surface level within the gap of the bulk material; the LUMO does not evolve into the conduction-band minimum. This surface nature causes the optical gaps of the larger diamondoids to lie below the bulk gap.

The surface nature of the LUMO is also responsible for some of the previous controversies in evaluating the energy of this state. The inset of Fig. 1(b) shows an example of the convergence of the electronic eigenvalues in a DFT-PBE calculation of $C_{10}H_{16}$ using a Gaussian basis. It shows the energy of the HOMO and LUMO calculated with the G03 code [20] using 6-31G*, 6-311G**, aug-ccp-vtz [22], and aug-ccp-vqz [22] basis sets. The energy of the LUMO decreases by almost 2 eV as more diffuse basis functions are added, while the HOMO energy stays approximately constant. If a localized basis set with insufficient flexibility to describe the diffuse character is used, the LUMO will be artificially localized close to the nanoparticle, increasing its kinetic energy and pushing up its energy. However, when the large aug-ccp-vtz [22] and aug-ccp-vqz [22] basis sets are used, the Gaussian DFT-PBE HOMO-LUMO gaps agree with the plane-wave results to within 0.01 eV.

The QMC calculations were performed with the CASINO [23] code using Slater-Jastrow [24] trial wave functions of the form $\Psi_T = D^{\uparrow}D^{\downarrow}\exp[J]$, where $D^{\uparrow}$ and $D^{\downarrow}$ are Slater determinants of up- and down-spin orbitals taken from DFT calculations and $\exp[J]$ is a Jastrow correlation factor, which includes electron-electron and electron-ion terms expanded in Chebyshev polynomials. The Jastrow factor was optimized using a standard variance-minimization scheme [24]. All the QMC optical gaps were calculated using diffusion Monte Carlo (DMC) calculations [24]. To converge the DMC total energies with respect to time step and population size, a time step of 0.02 a.u. was used and the target population was at least 640 configurations in each calculation. The ionic cores were represented by the same TM PBE pseudopotentials used in the DFT calculations. The effect on the QMC energies of using local-density approximation (LDA) or PBE functionals to generate the DFT orbitals was also tested. When the PBE functional and pseudopotentials were replaced with the LDA functional and pseudopotentials, the DFT and DMC gaps of $C_{29}H_{36}$ were reduced by 0.1 eV and 0.3(1) eV, respectively. The DFT and DMC optical gaps are therefore relatively insensitive to the choice of functional.

The optical gaps of the diamondoids were calculated as the difference in the DMC energy of the ground state and an excited state. The absorption of a photon creates an excited singlet state. The description of such a state requires two pairs of Slater determinants. However, for computational simplicity, we represented the excited state by replacing the HOMO in the spin-down Slater determinant with the LUMO. Within Ziegler's sum model for restricted Hartree-Fock states [25], the error incurred by adopting this mixed-state approach is equal to half the singlet-triplet splitting. This error is typically 0.1–0.2 eV in group-IV nanostructures of this size [26], which is small compared with the optical gaps. Previous QMC calculations of the optical gaps of Si nanoparticles [14] using this approach were shown to be in excellent agreement with *GW*-Bethe-Salpeter-equation (*GW*-BSE) calculations of the true singlet excitation energies.

To investigate the sensitivity of the QMC excitation energies to the choice of single-particle states, the excited-state calculations were repeated with three choices for the LUMO: (i) the unoccupied LUMO from a ground-state DFT calculation; (ii) the HOMO* occupied by the excited electron in a DFT calculation of an excited triplet; (iii) the HOMO* occupied by the excited electron in a DFT calculation of an excited mixed state. The DMC excited-state energies evaluated using (i) and (ii) were 0.3(1) eV lower than the energy evaluated using (iii), and therefore we conclude that the excitation energy is relatively insensitive to the choice of the DFT orbital used to represent the excited electron in the Slater determinant.

The DMC optical gaps of the diamondoids are given in Table I and are plotted against nanoparticle size in Fig. 1. DMC calculations do not suffer from the well-known DFT "band-gap problem," as they fully describe the interaction of the valence electrons with the electron excited into the LUMO by the absorption of a photon, so that electron-hole correlation is accounted for. The DMC optical gaps are significantly larger than the DFT HOMO-LUMO gaps, as was found for Si nanoparticles [14]. For example, the DMC optical gap of $C_{10}H_{16}$ is 7.61(2) eV, while the DFT-PBE

gap is 5.77 eV. Nevertheless, the DMC results confirm the qualitative trend for the size dependence of the gap predicted by DFT-PBE calculations. The DMC calculations predict that quantum confinement will be observed only in diamondoids smaller than 1 nm. The rapid decay of quantum confinement in diamond nanoparticles is consistent with the small exciton Bohr radius in diamond (1.6 nm), compared to Si (4.9 nm). The optical gap of $C_{66}H_{64}$ is below the bulk-diamond gap, as Raty *et al.* [7] predicted in their DFT study. These DMC optical-gap calculations support the interpretation of the x-ray absorption measurements in Ref. [7], which found no quantum confinement effects in 4 nm diamondoids.

To calculate the electron affinity (EA) and ionization potential (IP) of representative nanoparticles, DFT and QMC calculations were performed for the total energy differences $\mathrm{EA} = E_N - E_{N+1}$ and $\mathrm{IP} = E_{N-1} - E_N$, where E_N is the ground-state energy of a neutral molecule with N electrons. The trial wave functions for the E_{N+1} and E_{N-1} systems were constructed by adding and removing the orbitals corresponding to the LUMO and the HOMO from the down-spin Slater determinant.

The DMC electron affinities and ionization energies of $C_{10}H_{16}$ and $C_{29}H_{36}$ are given in Table I. Both nanoparticles have a negative electron affinity [$-0.13(2)$ and $-0.29(6)$ eV, respectively]. In contrast to the optical gaps, where the DMC values are significantly larger than the DFT values, the DMC electron affinities agree well with the DFT values; for example, the DFT electron affinity of $C_{10}H_{16}$ is -0.128 eV. The NEA suggests that coating surfaces with diamondoids could be a simple and economic method of producing electron emitters.

Finally, we have studied the exciton binding energy, which is defined as the difference between the quasiparticle and optical gaps, for small diamondoids. For Si nanoparticles, QMC and *GW*-BSE calculations have found that the exciton binding is dramatically enhanced at the nanoscale due to the increased overlap of the electron and hole [27]. Surprisingly, the exciton binding energy of $C_{29}H_{36}$ is only 1.25(10) eV compared to 2.6 eV for the equivalent $Si_{29}H_{36}$ nanoparticle [27]. The origin of this reduced exciton binding can again be traced to the different nature of the LUMO in C and Si nanoparticles. The delocalized LUMO in $C_{29}H_{36}$ [see Fig. 2(b)] has a much smaller dipole matrix element with the HOMO than the equivalent orbital in $Si_{29}H_{36}$, reducing the exciton binding.

In conclusion, we have performed DFT and QMC calculations of the single-particle and optical gaps of H-terminated C nanoparticles. Our DFT and QMC calculations confirm the predictions of Raty *et al.* [7] that quantum confinement effects disappear in nanoparticles larger than 1 nm. We have shown that the LUMO of H-terminated C nanoparticles is a delocalized surface state, in contrast to Si and Ge nanoparticles, where the LUMO is core confined. The delocalized nature of the LUMO results in an anomalously small exciton binding, a negative electron affinity, and optical gaps of larger nanoparticles that are below the bulk gap.

We thank J. Grossman for performing the Gaussian DFT calculations, and J.-Y. Raty, T. van Buuren, and J. Dahl for helpful conversations. N. D. D. acknowledges financial support from the LLNL Summer Institute on Computational Chemistry and Materials Science. This work was performed under the auspices of the U.S. Department of Energy by the University of California, Lawrence Livermore National Laboratory under Contract No. W-7405-Eng-48. N. D. D. and R. J. N. acknowledge financial support from EPSRC, U.K. Computational resources were provided by LLNL and the Cambridge-Cranfield HPCF.

*Electronic address: williamson10@llnl.gov

[1] W. Wilson, P. Szajowski, and L. Brus, Science **262**, 1242 (1993).
[2] G. Medeiros-Ribeiro *et al.*, Science **279**, 353 (1998).
[3] J. E. Dahl, S. G. Liu, and R. M. K. Carlson, Science **299**, 96 (2003).
[4] F. Himpsel *et al.*, Phys. Rev. B **20**, 624 (1979).
[5] M. J. Rutter and J. Robertson, Phys. Rev. B **57**, 9241 (1998).
[6] Y. K. Chang *et al.*, Phys. Rev. Lett. **82**, 5377 (1999).
[7] J.-Y. Raty *et al.*, Phys. Rev. Lett. **90**, 037401 (2003).
[8] S. Hosokawa *et al.*, J. Electron Spectrosc. Relat. Phenom. **137**, 235 (2004).
[9] A. Barnard, S. Russo, and I. Snook, Phys. Rev. B **68**, 073406 (2003).
[10] G. Lee *et al.*, Phys. Rev. Lett. **91**, 265701 (2003).
[11] N. Park *et al.*, Phys. Rev. B **69**, 195411 (2004).
[12] G. McIntosh, M. Yoon, S. Berber, and D. Tománek, Phys. Rev. B **70**, 045401 (2004).
[13] Y. Tang *et al.*, Chem. Phys. Lett. **372**, 320 (2003).
[14] A. J. Williamson *et al.*, Phys. Rev. Lett. **89**, 196803 (2002).
[15] M. D. Towler, R. Q. Hood, and R. J. Needs, Phys. Rev. B **62**, 2330 (2000).
[16] J. P. Perdew, K. Burke, and M. Ernzerhof, Phys. Rev. Lett. **77**, 3865 (1996).
[17] F. Gygi, The GP Code LLNL, 2004.
[18] F. Gygi, The QBox Code LLNL, 2004.
[19] The ABINIT code is a common project of the Université Catholique de Louvain, Corning, Inc., and other contributors, http://www.abinit.org, 2004.
[20] M. Frisch, computer code GAUSSIAN 03, Revision A.1, Gaussian, Inc., Pittsburgh, PA, 2003.
[21] A. Yoffe, Adv. Phys. **51**, 799 (2002).
[22] T. J. Dunning, J. Chem. Phys. **90**, 1007 (1989).
[23] R. J. Needs *et al.*, *CASINO version 1.6 User Manual* (University of Cambridge, Cambridge, 2002).
[24] W. M. C. Foulkes *et al.*, Rev. Mod. Phys. **73**, 33 (2001).
[25] T. Ziegler, A. Rauk, and E. J. Baerends, Theor. Chim. Acta **43**, 261 (1977).
[26] D. Prendergast *et al.*, J. Am. Chem. Soc. **126**, 13 827 (2004).
[27] L. Benedict *et al.*, Phys. Rev. B **68**, 085310 (2003).